Author version

Published as:

Yan, J., Sperry, M., Kamensky, D., & Hwang, J. T. (2021). Dynamic topology optimization of battery packs for eVTOL aircraft under time-dependent loading. In AIAA AVIATION 2021 FORUM (Paper No. AIAA 2021-3068). https://doi.org/10.2514/6.2021-3068

BibTeX for this reference:

https://lsdolab.github.io/lsdo-publications/publication/yan2021dynamic/

```
@inproceedings{yan2021dynamic,
  author = {Jiayao Yan and Mark Sperry and David Kamensky and John T. Hwang},
  title = {Dynamic topology optimization of battery packs for eVTOL aircraft under
    time-dependent loading},
  booktitle = {AIAA AVIATION 2021 FORUM},
  year = {2021},
  doi = {10.2514/6.2021-3068},
  url = {https://doi.org/10.2514/6.2021-3068}
}
```

Dynamic topology optimization of battery packs for eVTOL aircraft under time-dependent loading

Jiayao Yan*, Mark Sperry†, David Kamensky‡, and John T. Hwang§
University of California, San Diego, La Jolla, CA, 92093

Electric air taxis are envisioned to enable a new form of aviation in dense, urban locations. One of the feasibility barriers is the limited range due to the much lower energy densities that batteries have compared to fuel. A promising research direction to overcome this bottleneck is the use of multi-functional battery packs that dissipate heat but also carry structural loads. Here, we propose a scalable approach with automated derivative computation to design a battery pack of an eVTOL aircraft considering the power profile in takeoff, which is presumed to be the sizing condition. The problem uses a multi-fidelity submodel consisting of an equivalent circuit model to represent battery cells and a high-fidelity dynamic thermoelastic submodel of the battery pack. First, a steady-state topology optimization problem is solved based on the maximum heat output of the battery cells, computed from the aircraft power profile. Second, a dynamic topology optimization problem is solved based on the transient portion of the transition from liftoff to forward flight. Compared to the steady-state topology optimization, a 9.94% reduction in time-averaged compliance is obtained with the dynamic topology optimization.

I. Introduction

The design of electric vertical takeoff and landing (eVTOL) aircraft has been the target of growing interest in recent years for both industry and academia, with the vision of enabling rapid on-demand mobility in dense, congested urban locations [1]. The electric propulsion system is a critical component for the performance and safety of eVTOL aircraft. Compared to a conventional fuel-powered aircraft, electric propulsion benefits from higher energy-conversion efficiency, the absence of local emissions, greater reliability, lower noise, and the possibility of distributed propulsors—which provides redundancy. However, there are three key limiting factors related to the battery technology: the energy density of the battery, charging rate, and the cycle life [2].

When sizing the battery, thermal modeling is important to ensure the avoidance of thermal runaway, which is a catastrophic failure condition. The battery sizing also has a large impact on operating cost. As batteries are expected to have a cycle life in the neighborhood of 1000 cycles, their per-mission amortized cost is expected to be larger than that of the airframe and avionics combined [3]. As a result, the batteries must be carefully sized to not only achieve the required range, but provide as large a cycle life as possible. Battery cycle life, in turn, is highly dependent on peak thermal loading [4].

A key consideration is to ensure sufficient battery energy density to meet range requirements. Compared to traditional aircraft designs, this is a major challenge because the energy density of batteries is multiple orders of magnitude lower than that of fuel. This motivates the consideration of load-carrying battery packs that reduce the aircraft empty weight by integrating energy storage and structural components of the airframe. Given the aforementioned importance of battery cycle life, these load-carrying battery packs must be designed considering both structural and thermal loading.

Recent work has applied topology optimization to this design problem. Kambampati et al. [5] performed topology optimization of a battery pack with 25 cells using a steady-state thermoelastic model. They found that thermal and stress constraints are active for the design problem they considered, which establishes the need to use a coupled multiphysics model. The steady-state assumption leads to a conservative result because the time-dependent loading in actual conditions can be exploited to achieve feasible designs with even greater structural efficiency.

Here, we explore this possibility by performing dynamic topology optimization of battery packs considering time-dependent loading. In addition, we aim to achieve a general, modular, and easily reconfigurable implementation—therefore, we desire a methodology in which the derivative computation is fully automated. We implement our

*Ph.D. Student, Department of Mechanical and Aerospace Engineering, AIAA Student Member.
†Ph.D. Student, Department of Mechanical and Aerospace Engineering
‡Assistant Professor, Department of Mechanical and Aerospace Engineering.
§Assistant Professor, Department of Mechanical and Aerospace Engineering, AIAA Member.

optimization such that the derivative computation is fully automated, using an open-source optimization framework with modular architecture and automatic total derivative computation (OpenMDAO) [6], and a high-performance partial differential equation solver with symbolic partial derivative computation (FEniCS) [7]. In addition, our ODE solver uses general linear method with automatic calculation of the adjoint derivatives, so that the numerical method for the solution of the ODE is easily switchable.

Since we consider a time-dependent aircraft power profile, it is necessary to consider a battery cell model that can determine the cell heat flux from the demanded power. For the battery cell, we use an equivalent circuit model that approximate open-circuit voltage, internal resistance, and other battery properties as a function of state-of-charge and the cell temperature. The use of an equivalent circuit model and a battery pack thermoelastic model introduces two-way coupling between the cell and pack models. However, in this work, we make the assumption that the coupling is only one-way, meaning all the heat generated by the cells is dissipated via the battery pack.

There are two main objectives of this work:

1) We present a methodology for multi-physics dynamic topology optimization with fully automated derivative computation.
2) We compare the results of steady-state topology optimization to one-way coupled, dynamic topology optimization (mass minimization with temperature constraints) considering the takeoff of an eVTOL aircraft.

The remainder of this paper is organized as follows. Section II reviews the current state of battery pack modeling approaches, density-based topology optimization overview, and previous work in topology optimization using a modular approach. Section III summarizes the use of FEniCS, OpenMDAO, and an ODE solver using general linear method with automatic unsteady adjoint calculation. Section IV describes the battery cell and the battery pack submodels, respectively, while Section V introduces the formulation of the optimization problem. Section VI then introduces the optimization results. Section VII draws conclusions and outlines future work.

II. Background

A. Battery modeling approach

There are three main disciplines involved in modeling the battery packs of eVTOL aircraft: thermal analysis, elasticity, and electrochemistry. Previous work mainly used equivalent circuit models [8, 9] and pseudo-2D models [4] to model the electrochemistry at the battery pack level. The equivalent circuit model has relatively low fidelity but high computational efficiency, suitable for large-scale optimizations. Pseudo-2D models at the continuum scale model the solid and liquid diffusion, and thus provides the information within a battery cell. However, additional efforts are needed to generalize cell-level model to a battery-pack level model containing large numbers of battery cells.

Prior work in battery pack optimization is mostly at the cell level [10]. At the battery-pack level, Kambampati et al. [5] performed topology optimization using a battery-pack steady-state thermoelastic model with a constant heat flux term representing the battery cells. However, dynamic models are required to predict the battery performance and thermal limits based on time-dependent loading obtained from realistic eVTOL mission profiles. Sun et al. [11] presented a multi-fidelity simulation to predict the dynamic behavior of the battery pack using a combination of 3D finite element (FE) models and equivalent circuit models for the thermal modeling and the electrochemistry. Their work also suggested a potential way to model the electrochemistry and thermoelasticity with a computationally efficient multi-fidelity approach, bringing the possibility of applying large-scale multidisciplinary design optimization (MDO) to battery packs with time-dependent analysis.

B. Density-based topology optimization

Topology optimization is a numerical approach that designs the material layouts in a given design domain to improve their performance by minimizing an objective function [12, 13]. Recent advances widened the application of topology optimization to many other fields involving multiphysics, such as thermoelasticity [14, 15], fluid-structure interaction [16, 17], and acoustic-structure interaction [18–20]. The most common approaches for topology optimization are the level-set method (LSM) [21, 22] and density-based methods [23–25].

Here, we review density-based methods as it is used in our work. The general formula of density-based topology optimization is

$$
\begin{aligned}
\textbf{minimize} \quad & f \\
\textbf{with respect to} \quad & \boldsymbol{\rho}, \\
\textbf{subject to} \quad & \boldsymbol{R}(\boldsymbol{u}, \tilde{\boldsymbol{\rho}}) = 0 \\
& \int_{\Omega} \rho \, d\Omega = \text{constant} \\
& \rho_{\min} < \boldsymbol{\rho} \leq 1,
\end{aligned}
\tag{1}
$$

where f is the objective function; $\boldsymbol{\rho}$ is density vector, which is a scalar on each element; ρ is a density function on domain Ω; $\boldsymbol{R}$ is the assembled residual vector; $\rho_{min} > 0$ is a small constant to prevent singularities in the Jacobian of $\boldsymbol{R}$. Having a density value ρ close to zero means the region is void, while ρ close or equal to one means the region is occupied with material.

Filtering and penalization are two major steps that are necessary to ensure a valid and manufacturable solution for the density-based topology optimization. The use of a filter prevents numerical instabilities and checkerboard patterns in the optimized topology. A commonly used example is a linear density filter that averages the neighboring densities by taking a conic weight [26]. After the filtering step, the filtered density needs to be penalized to encourage them to converge to either zeros or ones. Two of the most commonly used density-based methods are the Solid Isotropic Material with Penalization (SIMP) method and the Rational Approximation of Material Properties (RAMP) method [27].

C. Prior work in topology optimization using a modular approach

Prior work implemented topology optimization in a modular way using OpenMDAO. Chung et al. [28] presented both the SIMP method and the LSM in OpenMDAO. They demonstrated the modularity and reusability of the optimization approach by assembling a parametric level-set method using the building blocks from the SIMP methods with minor changes. They tested their approach using a 2D cantilever beam linear elastic model. However, there is a chance to further explore the benefits of using an MDO framework, such as giving users more options for selecting the governing partial differential equation (PDE) or extending the topology optimization model as one of the disciplines for MDO.

Another prior work presented a topology optimization toolbox called ATOmiCS—automated topology optimization in OpenMDAO using FEniCS [29]. ATOmiCS fully automates the derivative computation for gradient-based topology optimization. It automatically computes the partial derivatives using FEniCS Unified Form Language (UFL). The total derivatives are computed in OpenMDAO. ATOmiCS has been implemented as a general-purpose toolbox providing users with multiple options for the governing equations, solvers, penalization methods, the objective, and constraints. It has been applied to three case studies [29]: cantilever beam topology optimizations using linear and nonlinear elastic model, steady-state battery pack optimization using thermoelastic model, and a liquid crystal elastomer shape matching optimization using a modified directional strain model.

III. Methodology

This section expands on the methodology used in this work for dynamic topology optimization (shown in Fig. 1). First, we introduce the approach for topology optimization with fully automated derivative computation using OpenMDAO and FEniCS. Then, we present an introduction to our numerical integration method, which computes the outputs of the system and the derivatives of outputs with respect to the inputs using the adjoint method.

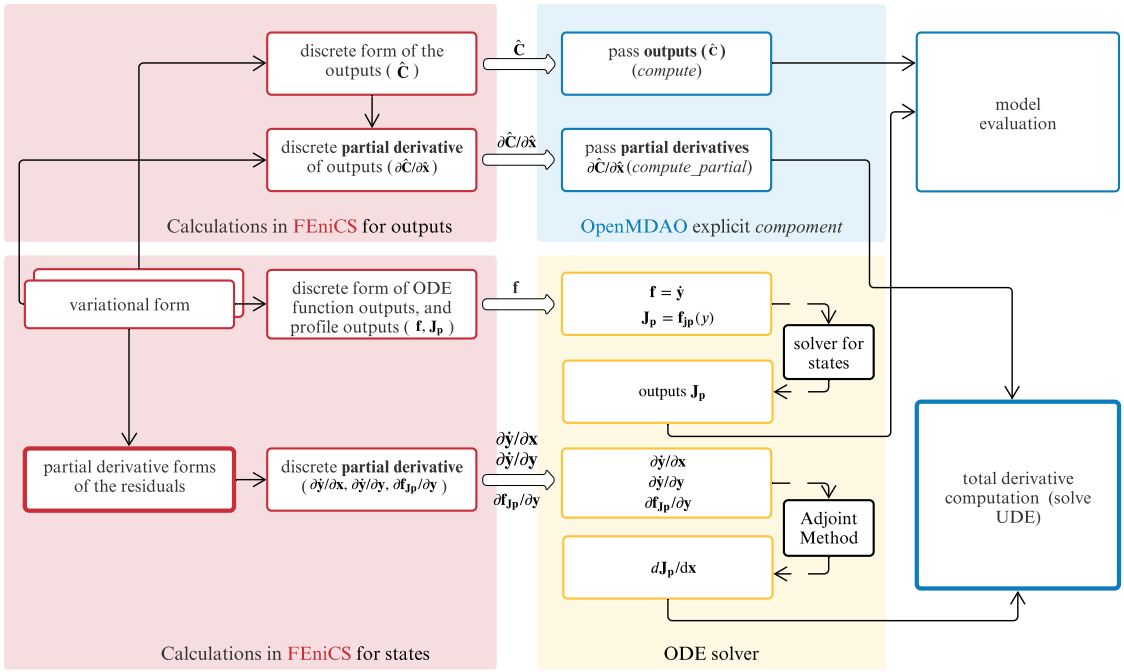

Fig. 1 Method for the computation of outputs, states, and the derivatives in OpenMDAO and FEniCS, and ODE solver with unsteady adjoint computation (wrapped in an OpenMDAO explicit *component*). The outputs that are not related to the states are denoted using $\hat{C}$; $\hat{x}$ and x are the inputs; f is the ODE function output vector; $\dot{y}$ is the ODE function; J_p represents the profile outputs that are related to the states; f_{Jp} is the profile outputs function; y represents the state vector.

A. Topology optimization with automated derivative computation

We use ATOmiCS for the topology optimization. It automates the derivative computation using OpenMDAO and FEniCS. The total derivatives are computed using OpenMDAO, which is an open-source software framework implemented in Python for large-scale gradient-based optimization [6]. It allows the construction of complex physical models involving multiple disciplines by decomposing the models into small units. Another key feature of OpenMDAO is its capability of automatically computing total derivatives by solving the unified derivatives equation (UDE) [30].

In addition, the partial derivatives are computed using FEniCS. The FEniCS user interface is based on Unified Form Language (UFL) [31], which is compiled into high-performance C++ code in the back end. UFL is composed of sublanguages for finite elements, expressions, and forms [7]. Those languages include integration over the domain and the boundary, computing the gradient of a function, and others such as basic linear algebraic operations. An important operator is called the *derivative* operator used to compute the symbolic Gâteaux derivatives [32].

The structure of this optimization problem is depicted in Fig. 2. The design variables are encapsulated in the density vector ($\boldsymbol{\rho}$). The density vector is first filtered using a distance-based linear filter imported from ATOmiCS. The filter computes the filtered density $\hat{\boldsymbol{\rho}}$ for unstructured meshes using a weighted average of densities in neighboring elements based on a KD tree search. Then, a penalization function penalizes the densities using the RAMP method implemented with FEniCS UFL operators. Next, the ODE function output ($\mathbf{f}$) and the profile outputs ($\mathbf{J_p}$) used to compute the constraint and objectives are computed by assembling FEniCS forms (shown in Fig. 1). The derivatives of the ODE function output with respect to the states and the input parameters ($\partial\dot{\mathbf{y}}/\partial\mathbf{y}$, $\partial\dot{\mathbf{y}}/\partial\mathbf{x}$), and the profile outputs with respect to the inputs ($\partial\mathbf{J_p}/\partial\mathbf{x}$) are computed symbolically using FEniCS derivative operator. Those partial derivatives are sent into the ODE solver for the solution of the states and the outputs.

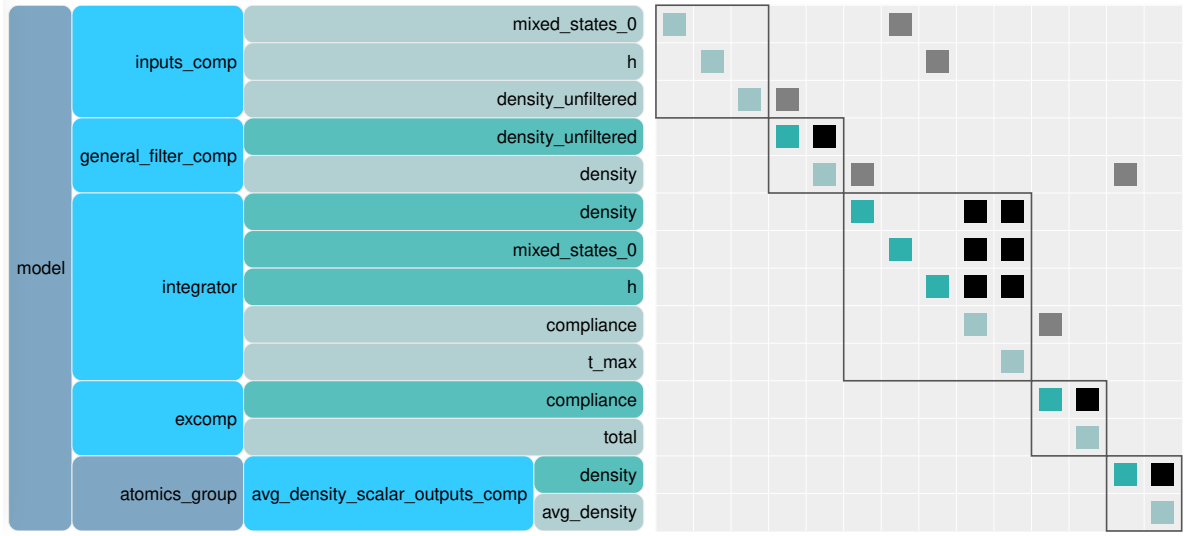

Fig. 2 n^2 diagram of the dynamic topology optimization problem.

B. ODE integration using general linear method with automatic unsteady adjoint calculation

We now introduce the procedure for the numerical integration of the dynamic thermoelastic problem and subsequently discuss the analytical computation of its derivatives for gradient-based optimization. Before discussing the solution method, we briefly establish the dynamic system. As described in Section III.A, the thermoelastic model described by (26) and (27) can be written as a differential equation of the form $\dot{\mathbf{y}} = f(\mathbf{y})$ where $y \in \mathbb{R}^S$.

For this problem, we incorporate Butcher's general linear method (GLM) [33]. The GLM is a general formulation of numerical ODE integration methods that have been used in ODE solvers in the past [34]. It can be written as

$$\begin{bmatrix} Y^{[n]} \\ y^{[n]} \end{bmatrix} = \begin{bmatrix} A \otimes \mathcal{I} & U \otimes \mathcal{I} \\ B \otimes \mathcal{I} & V \otimes \mathcal{I} \end{bmatrix} \begin{bmatrix} hF^{[n]} \\ y^{[n-1]} \end{bmatrix}, \tag{2}$$

where $y^{[n]}$ is the state vector at timestep n, $Y^{[n]}$ is the stage vector, $F^{[n]}$ is the vectorized ODE function applied to stage vector Y, h is the timestep size and A, B, U and V are unique coefficient matrices corresponding to a numerical method. $\mathcal{I}$ is an identity matrix of size S. The reason for the use of the GLM over other methods is due to the unique property that any linear multi-step or Runge-Kutta integration scheme can be represented by a unique set of matrices A, B, U and V. This allows rapid testing of different numerical integration methods by simply changing the coefficient matrices. Moreover, the GLM formulation poses a single, standardized equation that can be symbolically differentiated once, alleviating the need to differentiate each time integrator separately.

For this problem, the standard backward Euler method is used. There are two main benefits to this scheme: the guaranteed numerical stability of the solution due to implicit equations and the low cost from the fact that there is only one stage per time step. This is significant as the computation of $\dot{\mathbf{y}} = f(\mathbf{y})$ takes up the majority of the runtime.

To solve for the state $y^{[n]}$ at a given timestep, Eq. (2) is rearranged to produce

$$Y^{[n]} = \tilde{A}hF(Y^{[n]}) - \tilde{U}y^{[n-1]} \tag{3}$$

$$y^{[n]} = \tilde{B}h_nF^{[n]} + \tilde{V}y^{[n-1]}, \tag{4}$$

where $\tilde{A} = A \otimes \mathcal{I}$ with similar definitions for $\tilde{B}, \tilde{U}$, and $\tilde{V}$. At every new timestep, $y^{[n]}$ is substituted into $y^{[n-1]}$ to iteratively evaluate the state $y^{[n]}$ for $n = 1, \ldots N$ given initial conditions $y^{[0]}$.

As mentioned in Section III.A, we also introduce profile outputs $\mathbf{J_p}$ defined as

$$\mathbf{J_p} = \begin{bmatrix} \mathbf{J_p}^{[0]} \\ \vdots \\ \mathbf{J_p}^{[N]} \end{bmatrix} = \begin{bmatrix} f_{Jp}(y^{[0]}) \\ \vdots \\ f_{Jp}(y^{[N]}) \end{bmatrix} \tag{5}$$

where $f_{Jp} : \mathbb{R}^S \rightarrow \mathbb{R}^L$ and $L \leq S$. $\mathbf{J_p}^{[n]}$ is computed by evaluating $f_{Jp}(y^{[n]})$ after (4) at every timestep n. The motivation for the use of $\mathbf{J_p}$ instead of the full ODE state y is due to the extra states contained in y that are not needed. In summary, we solve the ODE problem using the GLM by applying (3) and (4) successively and computing $f_{Jp}(y^{[n]})$ at every timestep n to obtain the output $\mathbf{J_p}$.

We also introduce the analytical derivative computation of the outputs with respect to the inputs of the ODE system. The analytical derivatives are necessary for OpenMDAO's implementation of the UDE as described in Section III.A. For the thermoelastic problem, the input is the density vector $\boldsymbol{\rho}$. The outputs are generalized as $\mathbf{J_p}$ from the preceding paragraphs. The needed derivative of the ODE system is then $d\mathbf{J_p}/d\boldsymbol{\rho}$.

The adjoint method is used to evaluate the derivative. Because the thermoelastic problem has a greater number of inputs compared to the number of outputs, the adjoint method is one of the most efficient methods [35]. Using consistent notation with [35], we substitute the output with $\mathbf{J_p}$ and input with $\boldsymbol{\rho}$ to get

$$\frac{d\mathbf{J_p}}{d\boldsymbol{\rho}} = \frac{\partial F_J}{\partial \boldsymbol{\rho}} + \Psi^T \frac{\partial R}{\partial \boldsymbol{\rho}}, \tag{6}$$

$$-\frac{\partial R}{\partial r}^T \Psi = \frac{\partial F_J}{\partial r}, \tag{7}$$

where r and R represent the functions and variables of the intermediate steps by treating (3) and (4) at every timestep n as a series of coupled equations. F_J is the vectorized profile output function f_{Jp} applied across all states. A major issue with the adjoint method is the size of the Jacobian matrices. Because the Jacobian matrices include equations across all timesteps, they become large as N increases. To address this, we premultiply (6) with vector υ^T to form

$$\upsilon^T \frac{d\mathbf{J_p}}{d\boldsymbol{\rho}} = \upsilon^T \frac{\partial F_J}{\partial \boldsymbol{\rho}} + \tilde{\Psi}^T \frac{\partial R}{\partial \boldsymbol{\rho}}, \tag{8}$$

$$-\frac{\partial R}{\partial r}^T \tilde{\Psi} = \upsilon^T \frac{\partial F_J}{\partial r} \tag{9}$$

where $\tilde{\Psi}$ is simply $\Psi * \upsilon$. The only remaining large matrix is $(\partial R/\partial r)^T$ which has an upper block bidiagonal structure. This allows us to partition (8) and (9) into a system of three equations at every timestep N. After rearranging, we have

$$\upsilon^T \frac{d\mathbf{J_p}}{d\boldsymbol{\rho}} = \sum_{n=1}^{N} \left(-\tilde{\Psi}_a^{[n]} \tilde{A} \frac{\partial F^{[n]}}{\partial \boldsymbol{\rho}} - \tilde{\Psi}_b^{[n]} \frac{\partial F^{[n]}}{\partial \boldsymbol{\rho}} \right) \tag{10}$$

where $\tilde{\Psi}_b^{[n]}$ and $\tilde{\Psi}_b^{[n]}$ come from partitioning the adjoint vector $\tilde{\Psi}$ by

$$\tilde{\Psi} = \begin{bmatrix} \tilde{\Psi}^{[0]} \\ \vdots \\ \tilde{\Psi}^{[N]} \end{bmatrix}, \quad \tilde{\Psi}^{[n]} = \begin{bmatrix} \tilde{\Psi}_a^{[n]} \\ \tilde{\Psi}_b^{[n]} \\ \tilde{\Psi}_c^{[n]} \end{bmatrix}, \tag{11}$$

and

$$\begin{aligned} \tilde{\Psi}_c^{[n]} &= -\frac{\partial F_p}{\partial y^{[n]}} \upsilon_p^{[n]} + \tilde{U}^T \tilde{\Psi}_a^{[n+1]} + \tilde{V}^T \tilde{\Psi}_c^{[n+1]} \\ \tilde{\Psi}_b^{[n]} &= h\tilde{B}^T \tilde{\Psi}_c^{[n]} \\ -\left(\mathcal{I} - \tilde{A} h \frac{\partial F(Y_n)}{\partial Y_n} \right)^T \tilde{\Psi}_a^{[n]} &= \frac{\partial F(Y_n)}{\partial Y_n}^T \tilde{\Psi}_b^{[n]}. \end{aligned} \tag{12}$$

The full adjoint vector can be solved for by calculating $\tilde{\Psi}_c^{[n]} \rightarrow \tilde{\Psi}_b^{[n]} \rightarrow \tilde{\Psi}_a^{[n]}$ from $\tilde{\Psi}_c^{[n+1]}$ and $\tilde{\Psi}_a^{[n+1]}$ with $\tilde{\Psi}_c^{[N]} = 0$ and $\tilde{\Psi}_a^{[N]} = 0$. The left hand side of (10) is called the jacobian-vector product (JVP) and serves as the derivative for the ODE system [6]. The JVP measures the sensitivities of all outputs with respect to a unique set of inputs unlike the total derivatives which contain the independent sensitivities for all outputs and with respect to each independent input. The JVP is still compatible with gradient based optimization [6].

IV. Multi-fidelity model for battery pack optimization

To reduce the computational cost to a feasible level for large-scale MDO, we use a multi-fidelity approach (shown in Fig. 3), and perform topology optimization on the high fidelity thermoelastic submodel. The system is composed of an equivalent circuit model (ECM) for the battery cell, and a 2D dynamic thermoelastic model for the battery pack.

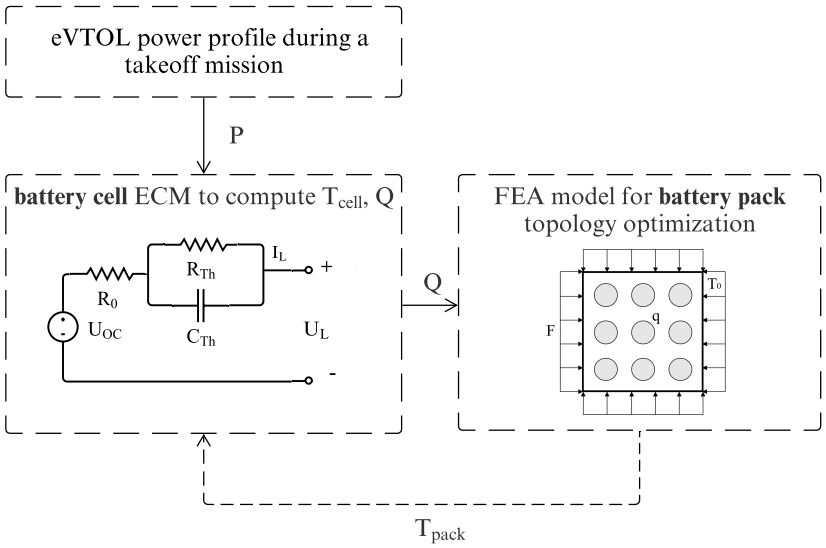

Fig. 3 Data flow between models of the mission profile, battery cells, and the battery pack.

First, we generate a mission profile for the dynamic part of the eVTOL aircraft takeoff phase using the model from Chauhan et al. [36]. The power output for each battery is scaled based on Airbus Vahana with two battery pack of 84 cells in series and 21 cells in parallel and a gross weight of 725 kg. Then, the power profile feeds into the equivalent circuit model (ECM). The ECM outputs the heat generated by one battery cell (Q). The heat output power Q is then converted to a heat flux term q to the battery pack submodel. For simplification, we assume a one-way coupling between the heat output profile of the battery cell. However, in reality, two-way coupling is present—the temperature of the battery pack (T_{pack}) influences the heat output and temperature of the battery cell. Finally, we perform topology optimization to minimize the compliance with a maximum temperature constraint on the 2D dynamic thermoelastic model of the battery pack.

A. Lumped parameter model for estimating the heat flux

We use an equivalent circuit model (ECM) to capture the dynamic heat output of the battery cells. The ECM expresses the dynamic of the battery cell using a lumped parameter resistor-capacitor (RC) block, which is also called a Thevenin model [37]. We assume a takeoff with little or no rest after a short mission is completed. Thus, the battery pack starts from a temperature of 55 °C and 80% state of charge. The maximum battery temperature to prevent thermal runaway is 70 °C. Thus, we set our highest temperature as 65 °C with a safety range of 5 °C. The battery parameters in this model are the open-circuit voltage (U_{OC}), the internal resistance (R_0), the Thevenin resistance (R_{Th}), and the Thevenin capacitance (C_{Th}).

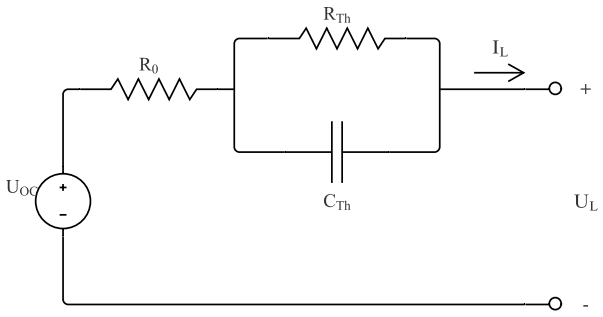

Fig. 4 The equivalent circuit model.

Data fitting for the battery We interpolate the battery parameters in (13) using the battery map from the data set provided in the work of Chin et al. [9]:

$$U_{\mathrm{OC}}, R_0, R_{\mathrm{Th}}, C_{\mathrm{Th}} = f(\mathrm{SoC}, T_{\mathrm{cell}}) \tag{13}$$

For the one-way coupling problem, we assume the battery cell temperature equals the maximum temperature of the battery pack implemented as a constraint in the topology optimization. We fit the battery parameters ($U_{\mathrm{OC}}, R_0, C_{\mathrm{Th}}$) using the regularized minimal-energy tensor-product splines (RMTS) method [38] from the Surrogate Modeling Toolbox [39]. R_{Th} is fitted using an exponentially decaying function with respect to the temperature and the SoC because of its high nonlinearity and the noise of the data.

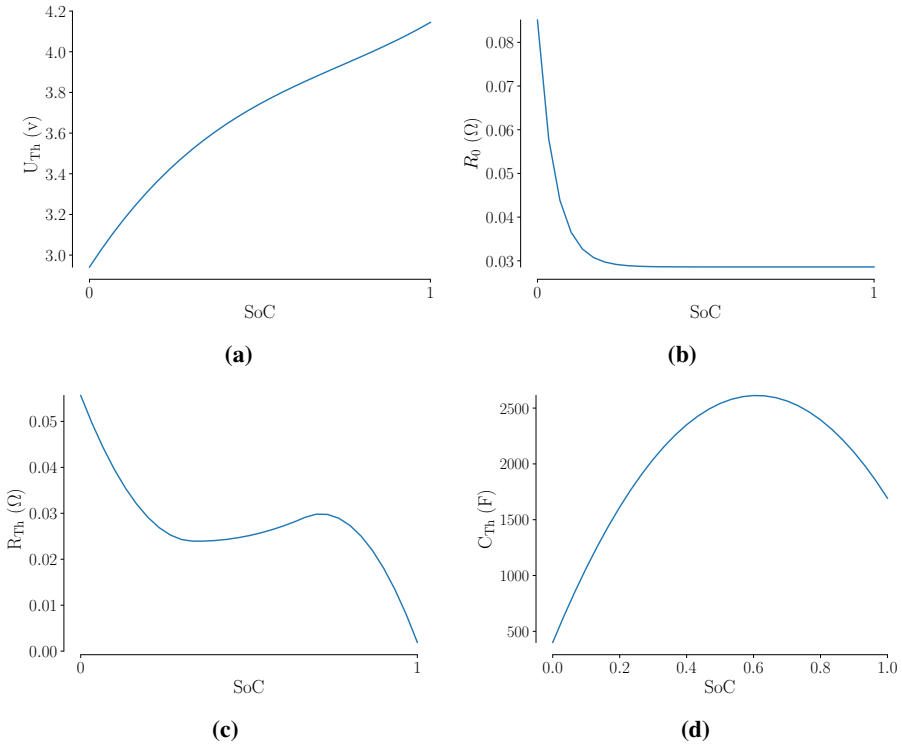

Fig. 5 Battery parameter curve fits. (a) Open-circuit voltage U_{OC}; (b) internal resistance R_0; (c) Thevenin resistance R_{Th}; (d)Thevenin capacitance C_{Th}.

Battery cell equivalent circuit model The ECM is implemented as a coupled ODE system with three states:

$$\begin{cases} \dfrac{\mathrm{d}SoC}{\mathrm{d}t} &= -\dfrac{I_L}{Q_{max} * 3600} \\ \dfrac{dU_{Th}}{dt} &= \dfrac{I_L - \frac{U_{Th}}{R_{Th}}}{C_{Th}} \\ \dfrac{dT_{\text{cell}}}{dt} &= \dfrac{P_{\text{net}}}{m_{\text{cell}} C_{\text{cell}}}, \end{cases} \tag{14}$$

where $Q_{max} = 3\,\text{Ah}$ is the maximum capacitance of the battery cell; P_{net}, P_{heat} are net output power and the heat dissipation power; η_{cell} battery cell efficiency; m_{cell} and C_{cell} are the mass and capacitance of the battery cell. U_{Th} is the Thevenin voltage, which relates to the open circuit voltage using the Kirchhoff's voltage law

$$U_L = U_{\text{OC}} - U_{\text{Th}} - I_L R_0, \tag{15}$$

where I_L is the line current. P_{net} is given by the difference between the heat generated by the battery cell P_{heat} and the heat dissipated to the battery pack Q

$$\begin{aligned} P_{\text{net}} &= P_{\text{heat}} - Q \\ &= I_L^2 (R_0 + R_{Th}) - \kappa A (T_{pack} - T_{cell}) \ . \end{aligned} \tag{16}$$

For the one-way coupled model, we assume $P_{\text{heat}} = Q$ for simplification, meaning the heat generated by the cells all dissipate into the battery pack. The input to the ECM is the power profile of the eVTOL given by

$$P = I_L U_L n_s n_p n_{\text{pack}}, \tag{17}$$

where the $n_s = 84$, $n_p = 21$, and $n_{\text{pack}} = 2$ are the number of serial cells, parallel cells, and number of battery pack units, respectively. The I_L in (14) can be expressed analytically as the solution of a quadratic equation in terms of the states and the power profile using (15) and (17):

$$I_{\text{L}} = \frac{(U_{\text{OC}} - U_{\text{Th}}) - \sqrt{(U_{\text{OC}} - U_{\text{Th}})^2 - 4R_0 \frac{P}{n_s n_p n_{\text{pack}}}}}{2R_0}. \tag{18}$$

The input and the output of the ECM is shown in Fig. 6. We interpolate 17 points from the transient portion of the takeoff phase for the 2D FEA model (Fig. 6b).

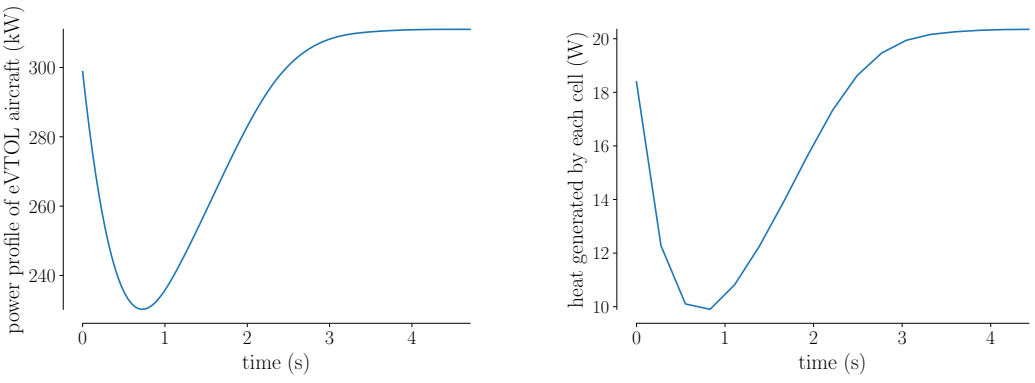

(a) **(b)**

Fig. 6 Input and outputs of the ECM. (a) power profile of an eVTOL aircraft during the dynamic part of the take-off process; (d) heat output Q of a battery cell.

B. Dynamic thermoelastic model for the battery pack

The PDE system we use to model thermoelasticity in batteries couples the dynamic heat equation

$$\rho T_0 \dot{s} + \nabla \cdot \mathbf{q} = 0 \tag{19}$$
$$\begin{cases} \mathbf{T} = T_0, & \text{on } \partial\Omega_{\text{pack}} \\ \mathbf{q} \cdot \mathbf{n} = q_0, & \text{on } \partial\Omega_{\text{cell}} \end{cases}$$

with quasi-static linear momentum balance

$$-\nabla \cdot \boldsymbol{\sigma} = 0\,, \tag{20}$$
$$\begin{cases} \mathbf{u} = \mathbf{0}, & \text{on } \partial\Omega_{\text{cell}} \\ \sigma\mathbf{n} = \mathbf{f}, & \text{on } \partial\Omega_{\text{pack}}\,, \end{cases}$$

where s is specific entropy, $\mathbf{q}$ is heat flux, $T_0 = 55\,^{\circ}\text{C}$ is a reference starting temperature, ρ is mass density, q_0 is the prescribed boundary heat flux related to the heat dissipation (Q) from the battery cell and contact area (A) of the pack and the cell, viz., $q_0 = Q/A$, $\boldsymbol{\sigma}$ is Cauchy stress, $\mathbf{n}$ is the outward-facing normal vector to $\partial\Omega$, $\partial\Omega_{\text{pack}}$ is the outside boundary of the pack, $\partial\Omega_{\text{cell}}$ is the union of cell boundaries, and $\mathbf{f} = 1.0 \times 10^6\ \text{Mm}^{-1}$ is a traction force applied on $\partial\Omega_{\text{pack}}$. We close this system of balance laws with the following constitutive models, to obtain a coupled PDE system for unknown temperature and displacement, T and $\mathbf{u}$:

$$\boldsymbol{\sigma} = \lambda \text{tr}(\boldsymbol{\varepsilon})\mathbf{I} + 2\mu\boldsymbol{\varepsilon} - \alpha(3\lambda + 2\mu)(T - T_0)\mathbf{I}\,, \tag{21}$$
$$\rho s = \rho s_0 + \frac{\rho C_\varepsilon}{T_0}(T - T_0) + \alpha(3\lambda + 2\mu)\text{tr}(\boldsymbol{\varepsilon})\,, \tag{22}$$
$$\mathbf{q} = -\kappa\nabla T\,, \tag{23}$$

where λ and μ are the Lamé parameters, $\mathbf{I}$ is the identity tensor, α is the thermal expansion coefficient, C_ε is the specific heat capacity at constant strain, κ is the thermal conductivity, s_0 is a reference value of specific entropy in the initial configuration, and $\boldsymbol{\varepsilon}$ is the symmetric gradient of $\mathbf{u}$. We simplify the pack into one that holds a three-by-three cell array with its boundary conditions, visualized in Fig. 7.

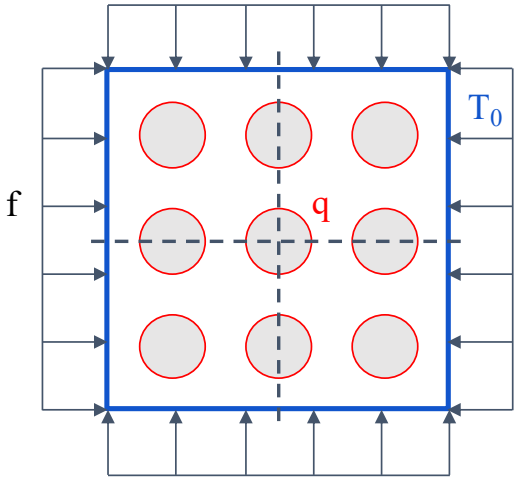

Fig. 7 Boundary conditions of the battery pack.

The system (19)–(20) can be cast in a weak form and discretized in space using the standard Bubnov–Galerkin finite element method. The implementation of this spatial discretization will be automated using FEniCS. The weak form of the coupled problem is: Find $(T, \mathbf{u}) \in S_T \times S_u$ such that, for all $(\hat{T}, \mathbf{v}) \in V_T \times V_u$,

$$\int_\Omega \rho T_0 \dot{s}\widehat{T}\,\text{d}\Omega + \int_\Omega \kappa\hat{\rho}\nabla T : \widehat{T}\,\text{d}\Omega - \int_{\partial\Omega_{\text{cell}}} q_0\widehat{T}\,\text{d}\partial\Omega_{\text{cell}} + \int_\Omega \boldsymbol{\sigma} : \nabla\mathbf{v}\,d\Omega - \int_{\partial\Omega_{\text{pack}}} \mathbf{f}\cdot\mathbf{v}\text{d}\partial\Omega_{\text{pack}} = 0\,, \tag{24}$$

where S_T and S_u are trial solution spaces for temperature and displacement, V_T and $\mathbf{V}_u$ are the corresponding test function spaces, $\hat{\rho}$ is the penalized density using the RAMP method, and the entropy rate $\dot{s}$ can be derived from (22) as

$$\rho \dot{s} = \frac{\rho C_\varepsilon}{T_0} \dot{T} + \alpha(3\lambda + 2\mu)\mathrm{tr}(\dot{\boldsymbol{\varepsilon}}) \ . \tag{25}$$

Relaxation for the lumped mass method The weak form (24) does not include time derivatives of $\mathbf{u}$, and would thus result in a differential–algebraic equation system after being discretized. To obtain an ODE system, we regularize the problem. First, we ignore the strain rate ($\dot{\varepsilon}$) term in (25), because the dynamics of the elastic problem are much faster than those of the thermal problem. Second, we add a viscous regularization term to the elasticity subproblem. The final regularized weak form is then: Find $(T, \mathbf{u}) \in S_T \times S_u$ such that, for all $(\hat{T}, \mathbf{v}) \in V_T \times V_u$,

$$\int_\Omega \left(\rho C_\varepsilon \dot{T} \widehat{T} + r \dot{\mathbf{u}} \cdot \mathbf{v} \right) \mathrm{d}\Omega + \int_\Omega \kappa \nabla T \cdot \nabla \widehat{T} \, d\Omega + \int_\Omega \boldsymbol{\sigma} : \nabla \mathbf{v} \, d\Omega = \int_{\partial\Omega_{cell}} q_0 \widehat{T} \, d\partial\Omega_{cell} + \int_{\partial\Omega_{\mathrm{pack}}} \mathbf{f} \cdot \mathbf{v} \, \partial\Omega_{pack} \ , \tag{26}$$

where $r > 0$ is a small constant regularization parameter. For finite-dimensional S_T, S_u, V_T, and V_u, this becomes the ODE system

$$\mathbf{M}\dot{\mathbf{y}} = \boldsymbol{\gamma}, \tag{27}$$

where $\mathbf{M}$ and $\boldsymbol{\gamma}$ are the mass matrix and right hand side vector, obtained from assembling the bilinear and linear terms of (26), and $\mathbf{y}$ is the vector of degrees of freedom in the mixed temperature–displacement approximation space. The mass matrix $\mathbf{M}$ is approximated via row-sum mass lumping, for computational efficiency and robustness.

V. Optimization formulation

We perform an optimization to minimize the compliance of the battery pack in (28). The objective is minimizing the average of compliance over all the time steps (n_t). The design variable is the density vector $\boldsymbol{\rho}$. The constraints of the optimization include a density constraint, a maximum temperature constraint, a constraint $\boldsymbol{\rho}_{\mathbf{cell}} = 1$ on the edges, and the elements surrounding the battery cells to preserve the key geometry, and a fixed volume constraint of 75%. The maximum temperature constraint is implemented using a constraint aggregation method called Kreisselmeier–Steinhauser function [40].

$$\begin{aligned}
\textbf{minimize} \quad & C = \frac{\sum_{i=1}^{n_t} \int_{\partial\Omega_{pack}} \mathbf{f} \cdot \mathbf{u} \, \mathrm{d}\partial\Omega_{pack}}{n_t} \ , \\
\textbf{with respect to} \quad & \boldsymbol{\rho}, \\
\textbf{subject to} \quad & 1 \times 10^{-5} < \boldsymbol{\rho} < 1 \\
& \mathrm{KS}(\mathbf{T}) \leq 65\,^\circ\mathrm{C} \\
& \boldsymbol{\rho}_{\mathbf{cell}} = 1 \\
& \int_\Omega \rho \, d\Omega = 75\%
\end{aligned} \tag{28}$$

VI. Results and discussions

A. Battery pack optimization with steady-state model

We perform steady-state topology optimization with a battery that has three-by-three battery cells on it. We consider the aluminium as the battery pack material. Table 1 lists the size of the domain and the material properties. We model one quarter of the domain with 1232 unstructured triangular elements and apply sliding boundary conditions to the symmetry plane. The heat flux is modeled q with the maximum value from the battery cell heat output profile Q. Thus, $q = 20.35\,\mathrm{W}$ in this optimization. The optimized topology is shown in Fig. 8. The compliance of the optimized structure is $117.64\,\mathrm{N/m}$. The maximum temperature is $65.00\,^\circ\mathrm{C}$ meaning the temperature constraint is active.

Table 1 Parameters for the steady-state and dynamic topology optimization problems

Size of the domain $(x \times y \times z)$	Young's Modulus $E_{\max}$ [Pa]	Thermal conductivity κ $[Wm^{-1}K^{-1}]$	Thermal expansion coefficient α $[K^{-1}]$
$0.06 \times 0.06 \times 0.05$	6.90×10^{10}	235	1.30×10^{-5}

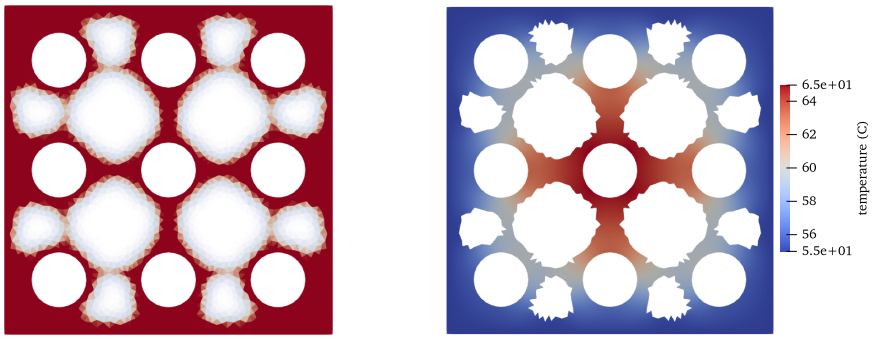

(a) **(b)**

Fig. 8 Optimization results with one-way coupled dynamic model. (a) optimized topology; (b) temperature field for the last time step.

B. Battery pack optimization with a one-way coupled dynamic model

We then perform a one-way coupled topology optimization applying the heat output profile (Figure. 6) from the ECM model to the battery pack finite element model using the same geometry and material as the steady-state model. We consider the dynamic part of the take-off process, which should have the highest heat output power, and thus it is used to approximate the sizing condition of the battery pack.

The optimized topology and the temperature field from the last time step are plotted in Fig. 9. The structure is similar to the one with a steady-state model because the maximum temperature constraint is active at the last time step (shown in Fig. 10), and the system almost reaches steady-state. The average compliance of the optimized structure is 107.00 N/m. At the last time step, the maximum temperature is 65.00 °C meaning the temperature constraint is active. We get a 9.94% reduction for the compliance compared to the steady-state solution. The benefits of using a dynamic model are inconclusive here because the sizing condition is at the last step, and the system almost reaches the steady-state.

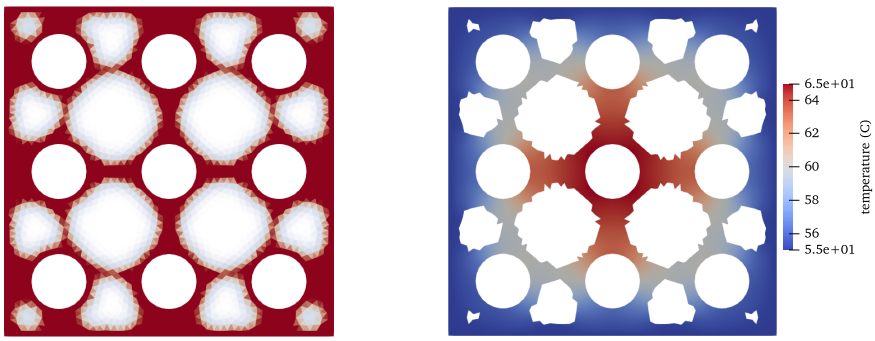

(a) **(b)**

Fig. 9 Optimization results with one-way coupled dynamic model. (a) optimized topology; (b) temperature field for the last time step.

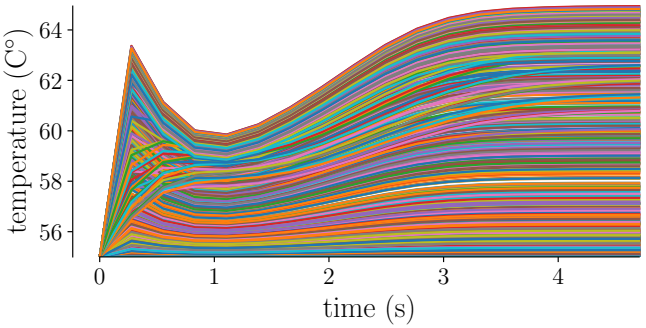

Fig. 10 Temperature history for the optimized topology with each state plotted as one line

VII. Conclusion and future work

In this work, we presented a modular topology approach for dynamic problems with automatic derivative computation. We applied this approach to a battery pack design problem with dynamic thermoelastic model considering the takeoff power profile of an eVTOL aircraft. In Section II, we reviewed battery pack modeling approaches, density-based topology optimization, and previous modular topology optimization implementations. Section III summarized the use of topology optimization approach with automatic derivative computation, and the numerical integration method for solving the ODE using a general linear method. Section IV introduced the multi-fidelity model. Section V introduced the formulation of the optimization problem. Section VI then discussed and compared the optimization results using a steady-state and a dynamic model.

The approach proposed in this work is applicable to general topology optimization problems with dynamic models without having users manually derive the derivatives, and thus scalable to complex models; In addition, the ODE solver we presented in this work applied general linear method with jacobian-vector products for the derivative computation, which standardized and reduced the effort of the derivative computation for unsteady problem using the adjoint method. Furthermore, this paper compared the dynamic topology optimization results with those using a steady-state model. Qualitatively the optimized topologies are similar in the problem considered; however, more investigation is required to make a conclusive statement of the need for dynamic topology optimization.

A promising avenue for future work is investigating the two-way coupled problem that approximates the heat transfer between the battery pack and battery cell using their temperature difference. Further investigation, for instance, different mission profiles, various battery pack layouts, also needs to be made to justify the benefits for dynamic topology optimization.

Acknowledgement

This material is based upon work supported by UCSD MAE First Year Fellowship. The authors would like to thank Dr. Shamsheer S. Chauhan for his valuable suggestions on selecting and generating the power profile for eVTOL aircraft.

References

[1] Bole, B., Daigle, M., and Gorospe, G., "Online prediction of battery discharge and estimation of parasitic loads for an electric aircraft," *ESC*, 2014.

[2] Holden, J., and Goel, N., "Fast-forwarding to a future of on-demand urban air transportation," *San Francisco, CA*, 2016.

[3] Brown, A., and Harris, W. L., "Vehicle Design and Optimization Model for Urban Air Mobility," *Journal of Aircraft*, Vol. 57, No. 6, 2020, pp. 1003–1013.

[4] Harrison, J., Charles, D., Zenker, J., and Frank, E., "Using Multi-physics System Simulation to Predict Battery Pack Thermal Performance and Risk of Thermal Runaway During eVTOL Aircraft Operations," *AIAA Propulsion and Energy 2019 Forum*, 2019, p. 4406.

[5] Kambampati, S., Gray, J. S., and Kim, H. A., "Level set topology optimization of structures under stress and temperature constraints," *Computers & Structures*, Vol. 235, 2020, p. 106265.

[6] Gray, J. S., Hwang, J. T., Martins, J. R., Moore, K. T., and Naylor, B. A., "OpenMDAO: An open-source framework for multidisciplinary design, analysis, and optimization," *Structural and Multidisciplinary Optimization*, Vol. 59, No. 4, 2019, pp. 1075–1104.

[7] Alnæs, M. S., Logg, A., Ølgaard, K. B., Rognes, M. E., and Wells, G. N., "Unified form language: A domain-specific language for weak formulations of partial differential equations," *ACM Transactions on Mathematical Software (TOMS)*, Vol. 40, No. 2, 2014, pp. 1–37.

[8] Hu, X., Li, S., and Peng, H., "A comparative study of equivalent circuit models for Li-ion batteries," *Journal of Power Sources*, Vol. 198, 2012, pp. 359–367.

[9] Chin, J. C., Schnulo, S. L., Miller, T. B., Prokopius, K., and Gray, J., "Battery Performance Modeling on Maxwell X-57," *AIAA Scitech 2019 Forum*, AIAA Aviation, American Institute of Aeronautics and Astronautics, 2019.

[10] Xue, N., Du, W., Gupta, A., Shyy, W., Sastry, A. M., and Martins, J. R., "Optimization of a single lithium-ion battery cell with a gradient-based algorithm," *Journal of The Electrochemical Society*, Vol. 160, No. 8, 2013, p. A1071.

[11] Sun, H., Wang, X., Tossan, B., and Dixon, R., "Three-dimensional thermal modeling of a lithium-ion battery pack," *Journal of Power Sources*, Vol. 206, 2012, pp. 349–356.

[12] Lazarov, B. S., Wang, F., and Sigmund, O., "Length scale and manufacturability in density-based topology optimization," *Archive of Applied Mechanics*, Vol. 86, No. 1-2, 2016, pp. 189–218.

[13] Bendsoe, M. P., and Sigmund, O., *Topology optimization: theory, methods, and applications*, Springer Science & Business Media, 2013.

[14] Guanghui, S., Chengqi, G., Dongliang, Q., Dongtao, W., Lei, T., and Tong, G., "An aerospace bracket designed by thermo-elastic topology optimization and manufactured by additive manufacturing," *Chinese Journal of Aeronautics*, Vol. 33, No. 4, 2020, pp. 1252–1259.

[15] Leader, M. K., Chin, T. W., and Kennedy, G., "Thermomechanical design of electric vehicle components with mission performance requirements using topology optimization," *AIAA Aviation 2019 Forum*, 2019, p. 3557.

[16] Lundgaard, C., Alexandersen, J., Zhou, M., Andreasen, C. S., and Sigmund, O., "Revisiting density-based topology optimization for fluid-structure-interaction problems," *Structural and Multidisciplinary Optimization*, Vol. 58, No. 3, 2018, pp. 969–995.

[17] Jenkins, N., and Maute, K., "An immersed boundary approach for shape and topology optimization of stationary fluid-structure interaction problems," *Structural and Multidisciplinary Optimization*, Vol. 54, No. 5, 2016, pp. 1191–1208.

[18] Hu, J., Yao, S., and Huang, X., "Topology optimization of dynamic acoustic–mechanical structures using the ersatz material model," *Computer Methods in Applied Mechanics and Engineering*, Vol. 372, 2020, p. 113387.

[19] Zhao, W., Chen, L., Chen, H., and Marburg, S., "Topology optimization of exterior acoustic-structure interaction systems using the coupled FEM-BEM method," *International Journal for Numerical Methods in Engineering*, Vol. 119, No. 5, 2019, pp. 404–431.

[20] Wang, X., Liu, B., and Wang, D., "Topology Optimization for Acoustic–Structure Interaction Systems Using the Model Reduction Method," *Journal of Vibration Engineering & Technologies*, Vol. 9, No. 2, 2021, pp. 341–353.

[21] Yaghmaei, M., Ghoddosian, A., and Khatibi, M. M., "A filter-based level set topology optimization method using a 62-line matlab code," *Structural and Multidisciplinary Optimization*, Vol. 62, No. 2, 2020, pp. 1001–1018.

[22] Laurain, A., "A level set-based structural optimization code using FEniCS," *Structural and Multidisciplinary Optimization*, Vol. 58, No. 3, 2018, pp. 1311–1334.

[23] Ferrari, F., and Sigmund, O., "A new generation 99 line Matlab code for compliance topology optimization and its extension to 3D," *Structural and Multidisciplinary Optimization*, Vol. 62, No. 4, 2020, pp. 2211–2228.

[24] Aranda, E., Bellido, J. C., and Donoso, A., "Toptimiz3D: A topology optimization software using unstructured meshes," *Advances in Engineering Software*, Vol. 148, 2020, p. 102875.

[25] Kim, C., Jung, M., Yamada, T., Nishiwaki, S., and Yoo, J., "FreeFEM++ code for reaction-diffusion equation–based topology optimization: for high-resolution boundary representation using adaptive mesh refinement," *Structural and Multidisciplinary Optimization*, 2020, pp. 1–17.

[26] Svanberg, K., and Svard, H., "Density filters for topology optimization based on the geometric and harmonic means," *10th world congress on structural and multidisciplinary optimization. Orlando*, 2013.

[27] Sigmund, O., and Maute, K., "Topology optimization approaches," *Structural and Multidisciplinary Optimization*, Vol. 48, No. 6, 2013, pp. 1031–1055.

[28] Chung, H., Hwang, J. T., Gray, J. S., and Kim, H. A., "Topology optimization in OpenMDAO," *Structural and multidisciplinary optimization*, Vol. 59, No. 4, 2019, pp. 1385–1400.

[29] Yan, J., Xiang, R., Kamensky, D., Tolley, T. M., and Hwang, T. J., "Topology Optimization with Automated Derivative Computation," *Manuscript submitted for publication*, 2021.

[30] Hwang, J. T., and Martins, J. R., "A computational architecture for coupling heterogeneous numerical models and computing coupled derivatives," *ACM Transactions on Mathematical Software (TOMS)*, Vol. 44, No. 4, 2018, pp. 1–39.

[31] Alnæs, M. S., "UFL: a finite element form language," *Automated Solution of Differential Equations by the Finite Element Method*, Springer, 2012, pp. 303–338.

[32] Dragomir, S. S., "Inequalities in terms of the Gâteaux derivatives for convex functions on linear spaces with applications," *Bulletin of the Australian Mathematical Society*, Vol. 83, No. 3, 2011, pp. 500–517.

[33] Butcher, J., "General linear methods," *Computers Mathematics with Applications*, Vol. 31, No. 4, 1996, pp. 105–112. https://doi.org/https://doi.org/10.1016/0898-1221(95)00222-7, URL https://www.sciencedirect.com/science/article/pii/0898122195002227, selected Topics in Numerical Methods.

[34] Hwang, J. T., and Munster, D., "Solution of ordinary differential equations in gradient-based multidisciplinary design optimization," *2018 AIAA/ASCE/AHS/ASC Structures, Structural Dynamics, and Materials Conference*, 2018. https://doi.org/10.2514/6.2018-1646.

[35] Martins, J., and Hwang, J., "Review and unification of methods for computing derivatives of multidisciplinary systems," *53rd AIAA/ASME/ASCE/AHS/ASC Structures, Structural Dynamics and Materials Conference 20th AIAA/ASME/AHS Adaptive Structures Conference 14th AIAA*, 2012. https://doi.org/10.2514/1.J052184.

[36] Chauhan, S. S., and Martins, J. R., "Tilt-wing eVTOL takeoff trajectory optimization," *Journal of Aircraft*, Vol. 57, No. 1, 2020, pp. 93–112.

[37] Plett, G. L., *Battery management systems, Volume I: Battery modeling*, Artech House, 2015.

[38] Hwang, J. T., and Martins, J. R., "A fast-prediction surrogate model for large datasets," *Aerospace Science and Technology*, Vol. 75, 2018, pp. 74–87.

[39] Bouhlel, M. A., Hwang, J. T., Bartoli, N., Lafage, R., Morlier, J., and Martins, J. R. R. A., "A Python surrogate modeling framework with derivatives," *Advances in Engineering Software*, 2019, p. 102662. https://doi.org/https://doi.org/10.1016/j.advengsoft.2019.03.005.

[40] Akgun, M., Haftka, R., Wu, K., and Walsh, J., "Sensitivity of lumped constraints using the adjoint method," *40th Structures, Structural Dynamics, and Materials Conference and Exhibit*, 1999, p. 1314.